Homochiral Coordination Polymers from Single Helices to Multiple Helices Controlled by Metal Ions①

XU Zhong-Xuan② HU Bang-Ping
LI Li-Feng XU Shi-Fei
(*School of Chemistry and Chemical Engineering, Zunyi Normal College, Zunyi* 563002, *China*)

ABSTRACT Helix as essential molecular chiral phenomenon at supramolecular level offers an affective method to study chiral characteristic of homochiral coordination polymers (CPs). Herein, two homochiral CPs $[Cd((R)\text{-}CBA)_2(3,5\text{-}DIT)]_n$ ((*R*)-H_2CBA = (*R*)-4-(1-carboxyethoxy) benzoic acid, 3,5-DIT = 3,5-di(1H-imidazol-1-yl)toluene, **1-*R***) and $[Zn((R)\text{-}CBA)(3,5\text{-}DIT)]_n$ (**2-*R***) were synthesized under hydrothermal conditions. In complex **1-*R***, only a helical chain was built by chiral ligands (*R*)-CBA^{2-}, ancillary ligands 3,5-DIT and Cd(Ⅱ) ions. After Cd(Ⅱ) ions were replaced by Zn(Ⅱ) ions under similar reaction system, Zn(Ⅱ), (*R*)-CBA^{2-} and/or 3,5-DIT formed six types of helices, resulting in complex **2-*R***. So, the metal ions played a key role in the construction of helical structures. Complexes **1-*R*** and **2-*R*** were also characterized by elemental analysis, PXRD, TGA, CD and UV-visible absorptions. In addition, complexes **1-*R*** and **2-*R*** exhibited different photoluminescence behaviors in solid sate compared to free ligand (*R*)-H_2CBA.

Keywords: homochiral coordination polymers, helical chain, metal ion effect, supramolecular framework;
DOI: 10.14102/j.cnki.0254–5861.2011–3139

1 INTRODUCTION

Helix as a special one-dimensional chiral form widely exists in biomolecules and performs crucial role in the natural world[1, 2]. For instance, double helix structure of DNA can store and transfer genetic information in organisms[3-5]. Therefore, the research of helical chiral compounds has scientific significance and applied importance. Homochiral CPs often contain absolute helix, offering an effective approach to understand the relationship of chirality and helicity[6-9]. Apart from delicate structures, homochiral CPs also possess promising applications in chiral separation, asymmetric catalysis, chiral recognition and so on, receiving a great amount of attention in recent years[10-13]. Some synthetic strategies, such as spontaneous resolution, asymmetric induction and chiral ligands, have been developed to prepare homochiral CPs[14-17]. Among them, using enantiopure organic compound as ligands to react with metal ions is the most direct and reliable synthetic method, so the design and selection of chiral ligands are a key factor in the synthesis of homochiral CPs.

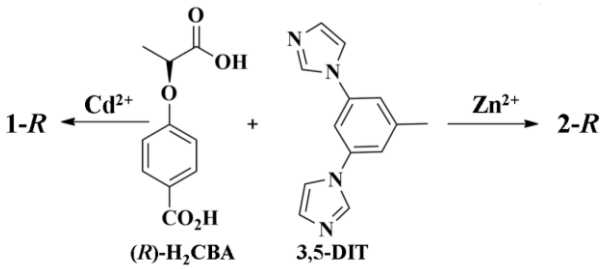

Scheme 1. Synthetic routes of complexes 1-*R* and 2-*R*

Received 22 February 2021; accepted 21 May 2021 (**CCDC 2061880 for 1-*R* and 2061881 for 2-*R***)
① This research was supported by the National Natural Science Foundation of China (No. 21761036)
② Corresponding author. E-mail: xuzhongxuan4201@163.com

Fortunately, nature has provided enormous amino and hydroxy acids as cheap and readily available synthons for homochiral CPs. However, their flexible skeletons and preferred chelating coordination modes are an obstacle to obtain Homochiral CPs. Therefore, utilizing organic moieties to modify amino and hydroxy acids is necessarily alternative[18-22]. Recently, chiral aromatic dicarboxylic ligands (*R*)-4-(1-carboxyethoxy)benzoic acid ((*R*)-H_2CBA) were synthesized by binding natural L-lactic acid to 4-hydroxybenzoic acid in our group[23]. Containing lactic and benzoic acid units, (*R*)-H_2CBA is a semi-rigid chiral ligand and has offered a new approach to synthesize homochiral CPs. Furthermore, selecting different metal ions to add in the reaction system is also a feasible method to obtain various homochiral CPs[24, 25].

According to the above mentioned synthetic strategy, we chose Zn(Ⅱ) and Cd(Ⅱ) ions to assemble with (*R*)-H_2CBA to build chiral CPs with the help of auxiliary ligand 3,5-di(1H-imidazol-1-yl)toluene (3,5-DIT), respectively (Scheme 1). As a result, $[Cd((R)\text{-CBA})(3,5\text{-DIT})]_n$ (**1-*R***) and $[Zn_2((R)\text{-CBA})_2(3,5\text{-DIT})_2]_n$ (**2-*R***) were successfully synthesized via similar hydrothermal methods. Single-crystal structure analysis revealed that (*R*)-CBA^{2-}, 3,5-DIT and Cd(Ⅱ) formed a chiral left-handed helical chain in **1-*R***, and correspondingly that (*R*)-CBA^{2-}, 3,5-DIT and Zn(Ⅱ) built six types of helixes in **2-*R***. Herein, we report their syntheses, structures, CD spectra, UV-visible absorption and fluorescence character.

2 EXPERIMENTAL

2. 1 General materials and methods

Chiral ligands (*R*)-H_2CBA were prepared according to the previously reported procedure[23]. The other chemicals were of reagent grade and directly used without further purification. Powder X-ray diffraction (PXRD) profiles were achieved on a Rigaku MiniFlex 600 diffractometer with Cu*Kα* (λ = 1.5406 Å) radiation (40 kV, 15 mA) from 5.00 to 50.00°. Thermogravimetric analyses (TGA) and the contents of C, H and N were measured though a NETSCHZ STA-F5 thermoanalyzer and a Perkin-Elmer 240C elemental analyzer, respectively. Circular dichroism (CD) data were obtained on a MOS-450 spectropolarimeter. UV-Vis absorption and fluorescent spectra were collected by a Shimadzu UV-3600 Plus spectrophotometer and a Hitachi FL-7000 fluorescence spectrophotometer, respectively.

2. 2 Synthesis of $[Cd((R)\text{-CBA})(3,5\text{-DIT})]_n$ (1-*R*)

The mixture of $Cd(NO_3)_2\cdot 4H_2O$ (90 mg, 0.3 mmol), (*R*)-H_2CBA (42 mg, 0.2 mmol), 3,5-DIT (0.3 mmol, 67 mg), NaOH (0.4 mmol, 16 mg) and 8 mL of water was kept stirring for 10 minutes, and then was sealed in a 10 mL Teflon-lined stainless autoclave and heated at 120 ℃ for 72 h. The colorless block crystals of **1-*R*** were isolated, washed with water and ethanol, and dried in air (Yield: 30% based on (*R*)-H_2CBA). Anal. Calcd. (%) for $C_{23}H_{23}N_4O_{6.50}Cd$: C, 48.31; H, 4.05; N, 9.80. Found (%): C, 47.24; H, 4.16; N, 9.68.

2. 3 Synthesis of $[Zn_2((R)\text{-CBA})_2(3,5\text{-DIT})_2]_n$ (2-*R*)

Complex **2-*R*** was prepared according to the above-mentioned procedure except $Cd(NO_3)_2\cdot 4H_2O$ (90 mg, 0.3 mmol) was replaced by $Zn(NO_3)_2\ 6H_2O$ (0.3 mmol, 90 mg). Colorless block crystals of **2-*R*** were obtained with a yield of 40% (based on (*R*)-H_2CBA). Anal. Calcd. (%) for $C_{46}H_{44}N_8O_{12}Zn_2$: C, 53.55; H, 4.30; N, 10.86. Found (%): C, 52.10; H, 4.22; N, 10.42.

2. 4 Single-crystal X-ray crystallography

Single crystal data of **1-*R*** and **2-*R*** were all collected by a Rigaku 003 CCD diffractometer with a Mo-*Kα* radiation (λ = 0.71073 Å). Their structures were solved by direct methods and refined by full-matrix least-squares analysis with SHELXT-2017 and SHELXL-2017 program packages on Olex2-1.2 software[24]. All hydrogen atoms attached to parent atoms were generated theoretically and treated as riding atoms with default parameters. Some selected bond lengths and angels are listed in Table 1.

Table 1. Selected Bond Lengths (Å) and Bond Angles (°)

1-*R*					
Bond	Dist.	Bond	Dist.	Bond	Dist.
Cd(1)–O(5)	2.477(3)	Cd(1)–N(4)^{a}	2.267(3)	Cd(1)–O(4)	2.250(3)
Cd(1)–O(2)^{b}	2.357(4)	Cd(1)–N(1)	2.244(3)	Cd(1)–O(1)^{b}	2.404(4)
N(4)^{b}–Cd(1)–O(5)	122.85(13)	N(4)^{b}–Cd(1)–O(2)^{a}	139.04(13)	N(4)^{b}–Cd(1)–O1^{a}	85.63(13)
N(4)–Cd(1)–O(5)	55.14(12)	O(4)–Cd(1)–N(4)^{b}	88.07(13)	O(4)–Cd(1)-O(2)^{a}	108.42(14)
O(4)–Cd(1)–O(1)^{a}	129.56(16)	O(2)^{a}–Cd(1)–O(5)	96.50(12)	O(2)^{a}–Cd(1)–O(1)^{a}	54.71(12)
N(1)–Cd(1)–O(5)	88.85(12)	N(1)–Cd(1)–N(4)^{b}	97.60(13)	N(1)–Cd(1)–O(4)	138.70(14)
N(1)–Cd(1)–O(2)^{a}	93.76(14)	N(1)–Cd(1)–O(1)^{a}	91.72(16)	N(1)^{a}–Cd(1)-O(5)	151.19(12)
2-*R*					
Bond	Dist.	Bond	Dist.	Bond	Dist.
Zn(1)–O(2)^{a}	1.996(2)	Zn(1)–O(5)	1.948(2)	Zn(1)–N(4)^{b}	2.028(2)
Zn(1)–N(1)	2.007(2)	Zn(2)–O(10)	1.942(2)	Zn(2)–N(8)^{3}	2.045(2)
Zn(2)–O(7)^{d}	1.992(2)	Zn(2)–N(5)	2.008(2)	O(2)^{a}–Zn(1)–N(4)^{b}	108.62(9)
O(2)^{a}–Zn(1)–N(1)	114.96(9)	O(5)–Zn(1)–O(2)^{a}	105.42(10)	O(5)–Zn(1)–N(4)^{b}	94.01(10)
O(5)–Zn(1)–N(1)	112.65(10)	N(1)–Zn(1)–N(4)^{b}	118.60(10)	O(10)–Zn(2)–N(8)^{c}	92.93(9)
O(10)–Zn(2)–O(7)^{d}	107.99(11)	O(10)–Zn(2)–N(5)	117.22(10)	O(7)^{d}–Zn(2)–N(8)^{c}	104.47(9)
O(7)^{d}–Zn(2)–N(5)	108.75(10)	N(5)–Zn(2)–N(8)^{c}	123.67(10)		

Symmetry transformation: a: –1+*x*, *y*, –1+*z*; b:1+*x*, *y*, –1+*z*; b: 1+*x*, *y*, –1+*z* for **1-*R***; a: 2–*x*, –0.5+*y*, 1–*z*; b: 1–*x*, –0.5+*y*, 2–*z*; c: –*x*, –0.5+*y*, 2–*z*; d: 1–*x*, –0.5+*y*, 2–*z* for **2-*R***

3 RESULTS AND DISCUSSION

3. 1 Structural descriptions for complexes 1-*R* and 2-*R*

Complex **1-*R*** crystallizes in triclinic *P*1 space group with absolute structural Flack factor of –0.057(18). In **1-*R***, each asymmetric unit is comprised of a Cd(Ⅱ) center, a deprotonated (*R*)-CBA^{2-} and a 1,4-BMIB ligand. The (*R*)-CBA^{2-} as κ_4-linker was linked by two Cd(Ⅱ) ions, while the Cd(Ⅱ) center adopted a slightly distorted octahedral bipyramidal configuration coordinated by four carbonyl O atoms from two (*R*)-CBA^{2-} and two imidazole N atoms from two 2,5-DIP (Fig. 1a). The existence of helical structure is the outstanding feature of complex **1-*R***. As shown in Fig. 1b, the Cd(Ⅱ) centers are connected by (*R*)-CBA^{2-} and 2,5-DIP ligands to form the left-handed helical chain along the *c*-axis (Fig. 1b). The adjacent helixes further constructed the helical 2,5-DIP-Cd-(*R*)-CBA layer (Fig. 1c). Finally, such 2*D* layers are packed together to form a 3*D* supramolecular framework of **1-*R*** (Fig. 1d). In the framework, each Cd(Ⅱ) center was connected by two 2,5-DIP ligands and two (*R*)-CBA^{2-} ligands, acting as a 4-connected node. Thereby, the **1-*R*** is a 4-connected sql net with a point symbol of ($4^4.6^2$) (Fig. 1e)[25].

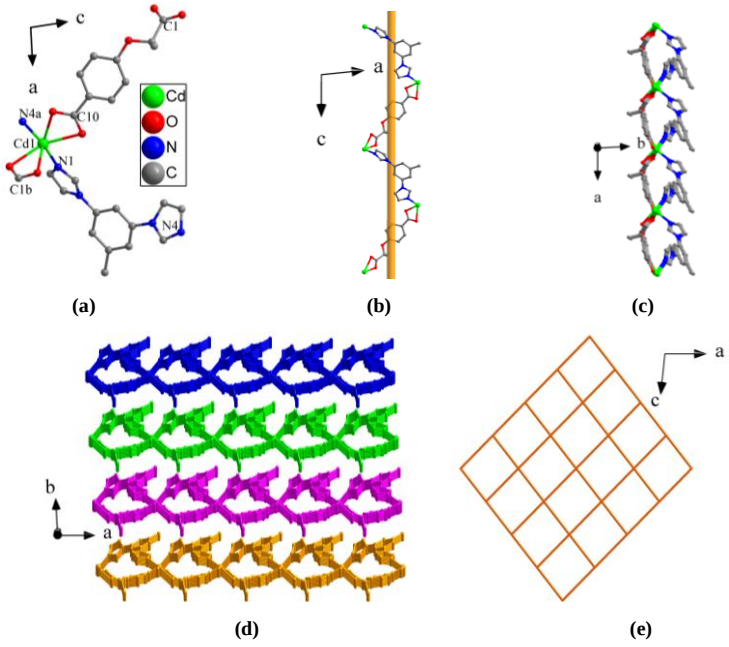

Fig. 1. Schematic illustration of complex 1-*R*: (a) coordination environment of Cd(Ⅱ) center; (b) right-handed helical chain formed by (*R*)-CBA^{2-}, 2,5-DIT and Cd(Ⅱ) ions; (c) 2*D* helical layer; (d) 3*D* supramolecular framework; (e) sql net

While Cd(Ⅱ) ions were replaced by Zn(Ⅱ) ions under the same condition, another chiral complex $[Zn_2((R)\text{-}CBA)_2(3,5\text{-}DIT)_2]_n$ (**2-*R***) was synthesized. X-ray crystallographic analysis revealed that **2-*R*** crystallizes in monoclinic space group $P2_1$ with absolute structural Flack factor of –0.006(3), respectively. There are two indepen- dent structural units in the asymmetric unit, and each structural unit is comprised of a Zn(Ⅱ) ion, a (*R*)-CBA^{2-} and a 3,5-DIT, where all Zn(Ⅱ) centers adopted a tetrahedral configuration coordinated by three carbonyl O atoms from two (*R*)-CBA^{2-} and two imidazole N atoms from two 3,5-DIT (Fig. 2).

Different from **1-*R*** with only one helix, complex **2-*R*** contains six types of helical chains. Thus, the helical structures are still the outstanding features of **2-*R***. The Zn1 and Zn2 ions were bridged by (*R*)-CBA^{2-} or 1,3-BMIB to form four types of left-handed helical chains in **2-*R*** along the *b* axis, respectively (Fig. 2a∼2d). Apart from the above helical chains, Zn1 and Zn2 ions were respectively connected by (*R*)-CBA^{2-} and 1,3-BMIB to form two other types of helical chains along the *a*-axis (Fig. 2e∼2f). Adjacent helical chains constructed two kinds of similar two-dimensional layers based on Zn1 or Zn2 ions (Fig. 2g). Finally, 2*D* layers are packed together to form a 3*D* supramolecular framework by hydrogen bonds (Fig. 3h and Table 2).

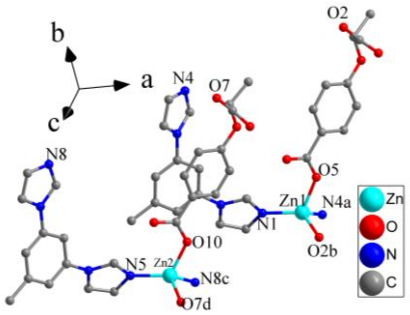

Fig. 2. Coordination environment of the Zn(Ⅱ) centers of 2-*R*

Table 2. Hydrogen Bond Geometry (Å, °) in Complex 2-*R*

D–H···A	D–H	H···A	D···A	D–H···A
O(1W)–H(1Wa)···O(4)	0.86(4)	1.97(4)	2.819(5)	168(5)
O(1W)–H(1Wb)···O(8)	0.85(5)	2.25(5)	3.093(5)	173(7)
O(2W)–H(2Wa)···O(8)	0.85	1.98	2.820(5)	172
O(1W)–H(2Wb)···O(8)	0.85	2.46	2.846(4)	108

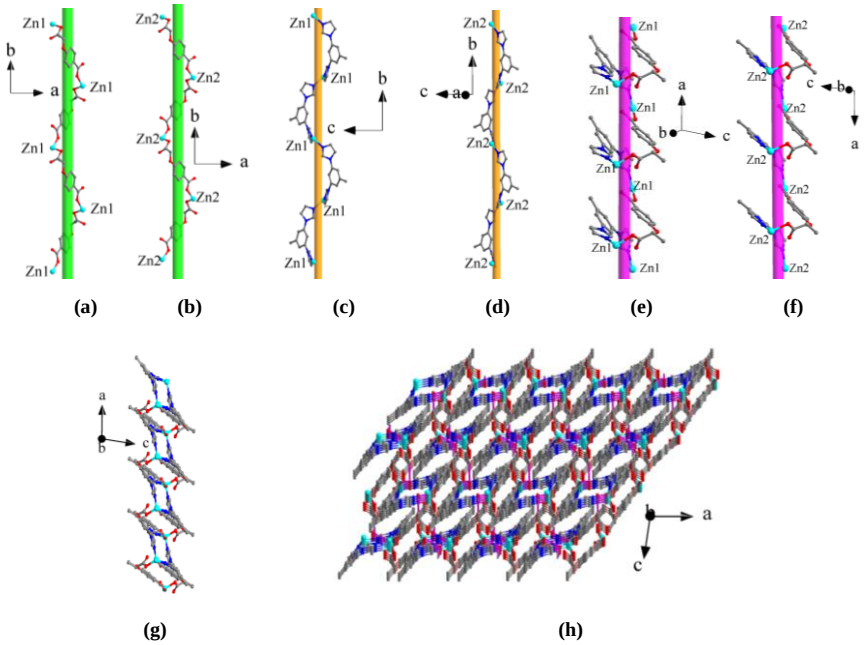

Fig. 3. Schematic illustrations of 2-*R*: (a) left-handed helix formed by Zn1 and (*R*)-CBA; (b) left-handed helix formed by Zn2 and (*R*)-CBA; (c) left-handed helix formed by Zn1 and 2,5-DIT; (d) left-handed helix formed by Zn2 and 2,5-DIT; (e) right-handed helix formed by Zn1, (*R*)-CBA and 2,5-DIT; (f) right-handed helix formed by Zn2, (*R*)-CBA and 2,5-DIT; g) 2*D* layer (constructed by helixes; (h) the 3*D* supramolecular framework based on 2*D* layers and hydrogen bonds

As far as complexes **1-*R*** and **2-*R*** are concerned, various frameworks were constructed by the same chiral ligands with different metal ions under the same hydrothermal condition. Helical structures existed in all the complexes, indicating that chirality of ligands can translate into the target frameworks to form helical chirality. Therefore, the chiral ligands played a key role in the synthesis of helical homochiral CPs. Furthermore, the introduction of different metal ions in reaction system is also an effective strategy to synthesize diversity homochiral CPs.

3. 2 PXRD and TG analyses

As displayed in Fig. 4a, the main peak positions in measured PXRD data of complexes **1-*R*** and **2-*R*** match very well with their simulated results from the single crystal data. The test results indicate that the crystal structures of **1-*R*** and **2-*R*** are truly representative of the crystal products. Additionally, thermal behaviors of complexes **1-*R*** and **2-*R*** were also studied by TGA to check their thermal stabilities (Fig. 4b). TGA curve of complex **1-*R*** shows a weight loss of 4.6% from room temperature to 210 ℃, which should be attributed to the release of guest water molecules (calculated, 4.5%). For complex **2-*R***, a weight loss of 3.3% appears between room temperature and 150 ℃, which should be also attributed to the release of guest water molecules (calculated, 3.5%). Over 290 ℃, the frameworks of **1-*R*** and **2-*R*** start to decompose until 800 ℃ without stopping.

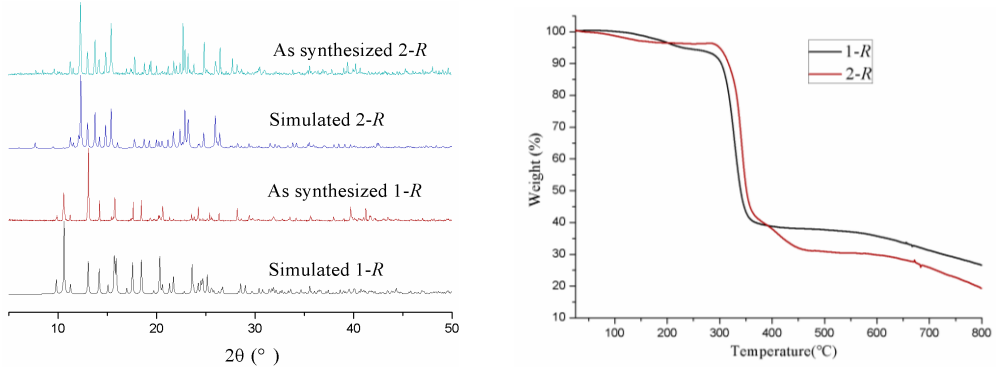

(a) **(b)**

Fig. 4. (a) PXRD patterns and (b) TGA curves of complexes 1-*R* and 2-*R*

3. 3 Circular dichroism

Although chirality of **1-*R*** and **2-*R*** has been confirmed by their space groups and absolute Flack factors, their solid-state circular dichroism (CD) spectra were still measured to further check their chiral characteristic (Fig. 5). Complex **1-*R*** has a broad positive CD signal about 224 nm, whereas complex **2-*R*** shows a strong positive Cotton effect with the peak located at around 233 nm and a weak negative Cotton effect CD signal at 264 nm. The above results from CD measurements once again indicated that **1-*R*** and **2-*R*** are both chiral complexes.

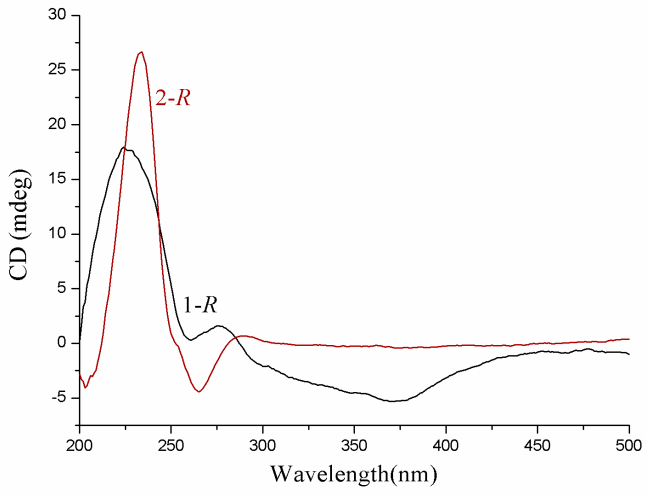

Fig. 5. Solid-state CD spectra of complexes 1-*R* and 2-*R*

3. 4 Solid UV-vis absorbing spectra and photoluminescent properties

The UV/vis spectra revealed that complexes **1-*R*** and **2-*R*** both have weak absorption bands from 400 to 900 nm and strong absorption bands in region of 200～400 nm (Fig. 6a). Upon excitation at 300 nm, complex **1-*R*** indicates a strong emission peak at about 330 nm. For **2-*R***, its emission spectrum excited at 297 nm exhibits strong emission peak at 357 nm. The solid-state photoluminescence property of free ligand (*R*)-H_2CBA was also investigated at room temperature to better understand the above emission bands. (*R*)-H_2CBA exhibits strong emission peak at 380 nm excited at 330 nm. As compared to (*R*)-H_2CBA, emission maxima of **1-*R*** and **2-*R*** both showed distinct blue-shift (Fig. 6b), which should be ascribed to intraligand (n–π* or π–π*) emission in **1-*R*** and **2-*R***.

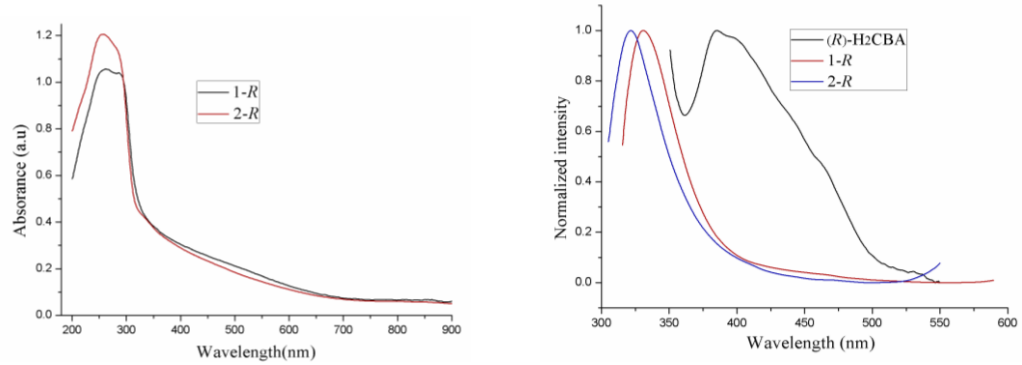

(a) **(b)**

Fig. 6. Solid UV-vis absorbing curves (a) and fluorescent emission spectra of 1-*R* and 2-*R*

4 CONCLUSION

In summary, two helical homochiral CPs have been successfully synthesized by using predesigned chiral lactate ligand (*R*)-H_2CBA to assemble with rigid auxiliary ligand 1,3-BMIB, Cd(II) or Zn(II) ions in similar conditions. Among them, Cd(II) centers, (*R*)-CBA^{2-} and 1,3-BMIB ligands formed a left-handed helical chain in complex **1**, while Zn(II) centers, (*R*)-CBA^{2-} and 1,3-BMIB ligands constructed six types of helixes in complex **2**. Herein, different coordination geometries between Cd(II) and Zn(II) ions leaded to different number of helices. This work can help us to further understand the metal effect in the synthesis of helical homochiral CPs .

REFERENCES

（1） Baumgartner, R.; Fu, H.; Song, Z.; Yao, L.; Cheng, J. Cooperative polymerization of α-helices induced by macromolecular architecture. *Nat. Chem.* **2017**, 9, 614–622.

（2） Arrata, I.; Barnard, A.; Tomlinson, D. C.; Wilson, A. J. Interfacing native and non-native peptides: using affimers to recognize α-helix mimicking foldamers. *Chem. Commun*. **2017**, 53, 2834–2837.

（3） Watson, J. D.; Crick, F. H. Molecular structure of nucleic acids: a structure for deoxyribose nucleic acid. *Nature* **1953**, 171, 737–738.

（4） Frankling, R. E.; Gosling, R. G. Molecular configuration in sodium thymonucleate. *Nature* **1953**, 171, 740–741.

(5) Wilkins, G. DNA: twin strands solved the structure. *Nature* **2013**, 496, 434–434.

(6) Bhattacharyya, A.; Ghosh, B. N.; Herrero, S.; Rissanen, K.; Jiménez-Aparicio, R.; Chattopadhyay, S. Formation of a novel ferromagnetic end-to-end cyanate bridged homochiral helical copper(II) Schiff base complex via spontaneous symmetry breaking. *Dalton Trans*. **2015**, 44, 493–497.

(7) Bisht, K. K.; Parmar, B.; Rachuri, Y.; Kathalikattil, A. C.; Suresh, E. Progress in the synthetic and functional aspects of chiral metal-organic frameworks. *CrystEngComm.* **2015**, 17, 5341–5356.

(8) Li, C.; Zhou, H.; Sun Y.; Guo, J.; Du, M. Controlled crystal transformations of a chiral conglomerate with heterotactic helical coordination arrays. *Cryst. Growth Des*. **2018**, 18, 4252–4256.

(9) Wu, X.; Zhang, H.; Xu, Z.; Zhang, J. Asymmetric induction in homochiral MOFs: from interweaving double helices to single helices. *Chem. Commun*. **2015**, 51, 16331–16333.

(10) Chang, C.; Qi, X.; Zhang, J.; Qiu, Y.; Li, X.; Wang, X.; Bai, Y.; Sun, J.; Liu, H. Facile synthesis of magnetic homochiral

metal-organic frameworks for “enantioselective fishing”. *Chem. Commun*. **2015**, 51, 3566−3569.

(11) Zhang, J.; Li, Z.; Gong, W.; Hang, X.; Liu, Y.; Cui, Y. Chiral DHIP-based metal-organic frameworks for enantioselective recognition and separation. *Inorg. Chem*. **2016**, 55, 7229−7232.

(12) Xia, Q.; Li, Z.; Tan, C.; Liu, Y.; Gong, W.; Cui, Y. Multivariate metal-organic frameworks as multifunctional heterogeneous asymmetric catalysts for sequential reactions. *J. Am. Chem. Soc*. **2017**, 139, 8259−8266.

(13) Hou, X.; Xu, T.; Wang, Y.; Liu, S.; Chu, R.; Zhang, J.; Liu, B. Conductive and chiral polymer-modified metal-organic framework for enantioselective adsorption and sensing. *ACS Appl. Mater. Interfaces* **2018**, 10, 26365−26371.

(14) Li, Y.; Wang, X.; Li, S.; Sun, H.; Jiang, Y.; Hu, M.; Zhai, Q. The power of heterometalation through lithium for helix chain-based noncentrosymmetric metal-organic frameworks with tunable second-harmonic generation effects. *Cryst. Growth Des*. **2017**, 17, 5634−5639.

(15) Xu, Y.; Li, X.; Wang, H.; Liu, H.; Chen, M.; Dou, Q. Synthesis, crystal structure and luminescence of one-dimensional homochiral terbium(III) coordination polymers. *Chin. J. Struct. Chem*. **2020**, 39, 1044−1050.

(16) Wang, N.; Fu, H.; Xie, T.; Shi, F.; Wang, T.; Yan, L.; Li, F. A zeolitic rho-type chiral metal-organic framework based on L-alanine. *Chin. J. Struct. Chem*. **2019**, 38, 963−969.

(17) Liu, Q.; Xiong, W.; Liu, C.; Wang, Y.; Wei, J.; Xiahou, Z.; Xiong, L. Chiral induction in the ionothermal synthesis of a 3*D* chiral heterometallic metal-organic framework constructed from achiral 1,4-naphthalenedicarboxylate. *Inorg. Chem*. **2013**, 52, 6773−6775.

(18) Yan, L.; We, C. Recent advances on porous homochiral coordination polymers containing amino acid synthons. *CrystEngComm.* **2014**, 16, 4907−4918.

(19) Chen, L.; Kang, J.; Cui, H.; Wang, Y.; Liu, L.; Zhang, L.; Su, C. Homochiral coordination cages assembled from dinuclear paddlewheel nodes and enantiopure ditopic ligands: syntheses, structures and catalysis. *Dalton Trans*. **2015**, 44, 12180−12188.

(20) Xu, Z.; Ma, Y. A pair of 3*D* homochiral coordination polymers with open channels constructed by lactic acid derivative ligands and *in-situ* formed anions. *Chin. J. Struct. Chem*. **2017**, 36, 671−678.

(21) Xu, Z.; Bai, X.; Men, Q. Two 3*D* Pillar-layered homochiral coordination complexes: syntheses, structures and properties. *Chin. J. Inorg. Chem*. **2020**, 36, 165−172.

(22) Li, M.; Chang, X.; Zeng, Y.; Song, H. Two concomitant polymorphs of homochiral Cu(Ⅱ) coordination compounds based on N-phthalyl-L-alanine: syntheses and crystal structures. *Chin. J. Inorg. Chem*. **2018**, 34, 83−91.

(23) Xu, Z.; Ma, Y.; Zhang, L. A couple of Co(II) enantiomers constructed from semirigid lactic acid derivatives. *Inorg. Chem. Commun*. **2016**, 73, 115−118.

(24) Xu, Z.; Bai, X.; Li, L.; Xu, S. Semi-conductive chiral Co−CPs with helixes based on lactic acid derivatives: synthesis, structures and photocatalyic properties. *J. Solid State Chem*. **2020**, 289, 121524-7.

(25) Xu, Z.; Shi, M. Two pairs of homochiral coordination polymers with helixes formed from lactic acid derivatives and rigid auxiliary ligands: syntheses, structures and properties. *Chin. J. Inorg. Chem*. **2019**, 35, 2346−2354.

(26) Sheldric, G. M. SHELXT-integrated space-group and crystal-structure determination. *Acta Cryst*. **2015**, C71, 3−8.

(27) Alexandrov, E. V.; Blatov, V. A.; Kochetkov, A. V.; Proserpio, D. M. Underlying nets in three-periodic coordination polymers: topology, taxonomy and prediction from a computer-aided analysis of the Cambridge Structural Database. *CrystEngComm.* **2011**, 13, 3947−3958.